Assembling Bi-, Tri- and Pentanuclear Complexes into Extended Structures Using a Desolvation Reaction: Synthesis, Structure, and Magnetic Properties of Manganese(III)−Schiff-Base−Hexacyanoferrate Polymeric Compounds and Their Derived Extended Structures

Hitoshi Miyasaka and Hidenori Ieda

Department of Chemistry, Faculty of Science, Kyushu University, Fukuoka 812, Japan

Naohide Matsumoto*

Department of Chemistry, Faculty of Science, Kumamoto University, Kurokami 2-39-1, Kumamoto 860, Japan

Nazzareno Re

Dipartimento di Chimica, Università di Perugia, I-06100 Perugia, Italy

Raffaella Crescenzi and Carlo Floriani*

Institut de Chimie Minérale et Analytique, BCH, Université de Lausanne, CH-1015 Lausanne, Switzerland

Received July 31, 1997

$[Mn(BS)(H_2O)]ClO_4$ and $[NEt_4]_3[Fe(CN)_6]$ react in methanol or ethanol to give a binuclear $[NEt_4]_2[\{Mn(BS)(S)\}\{Fe(CN)_6\}]$, **1**, three trinuclear $[NEt_4][\{Mn(BS)(S)\}_2\{Fe(CN)_6\}]$, **2**−**4**, and a pentanuclear $[Mn(BS)(S)]_4[Fe(CN)_6]ClO_4$, **5**, heterometal complex, depending on the nature of the quadridentate Schiff-base ligands and regardless of the stoichiometric ratio of the precursor components (BS = saldmen = *N*,*N*′-(1,1-dimethylethylene)bis(salicylideneiminato) dianion, S = H_2O for **1**; BS = *rac*-salmen = *rac*-*N*,*N*′-(1-methylethylene)bis(salicylideneiminato) dianion, S = MeOH for **2**; BS = *rac*-salcy = *rac*-*N*,*N*′-(1,2-cyclohexanediylethylene)bis(salicylideneiminato) dianion, S = MeOH for **3**; (*R*,*R*)-salcy = (*R*,*R*)-*N*,*N*′-(1,2-cyclohexanediylethylene)bis(salicylideneiminato) dianion, S = H_2O for **4**; BS = saltmen = *N*,*N*′-(1,1,2,2-tetramethylethylene)bis(salycylideneiminato) dianion, S = H_2O for **5**). Complexes **1** and **2** have been characterized by X-ray analyses. Complex **1** consists of a discrete CN-bridged Mn(III)−Fe(III) binuclear unit $[(H_2O)Mn(saldmen)Fe(CN)_6]^{2-}$ hydrogen-bonded into a one-dimensional chain structure. Complex **2** consists of a discrete centrosymmetric trinuclear unit $[(MeOH)Mn(salmen)Fe(CN)_6Mn(salmen)(MeOH)]^-$ hydrogen-bonded, thus forming a two-dimensional network with a repeating cyclic octamer $[-NC-Fe-CN-Mn-MeOH-]_4$ unit. Complexes **1**−**5** led to desolvated forms **1**′−**5**′. Some of these forms (**1**′−**3**′) show spontaneous magnetization according to an extended structure where the original magnetically isolated oligomeric forms now communicate with each other. In the case of **4**′ and **5**′, the desolvation probably occurs with a severe reorganization of the parent hydrogen-bonded extended structure, and hence, cooperative magnetic effects were not observed.

Introduction

Synthetic strategies of extended multidimensional structures have shown spectacular advances in the fields of supramolecular and condensed functional materials in recent years.[1] This is particularly true in the design of molecular ferromagnets,[2] in the theoretical approach to magnetism,[3] and in the functionalization of magnetic materials.[4] In our synthetic approach to magnetic materials, we have focused on the use of two complementary building blocks, one of them containing a bridging ligand and the other one vacant coordination sites.

In this context, we have been able to assemble $[Fe(CN)_6]^{3-}$ and $[Mn(H_2O)(salen)]^+$ into one-dimensional ferromagnetic, two-dimensional metamagnetic, and two-dimensional ferromagnetic materials.[5] They are made up of binuclear [MnFe], trinuclear [Mn_2Fe], and pentanuclear [Mn_4Fe] repeating units, respectively. The extended structures have been obtained in a single step, without the isolation of the intermediate polynuclear species. From a synthetic point of view, it would be particularly interesting to separate the assembling of the original mononuclear structure into polynuclear (first step) structures and then into the final extended ones (second step). In the present paper,

(1) (a) Abrahams, B. F.; Hoskins, B. F.; Michail, D. M.; Robson, R. *Nature* **1994**, *369*, 727. (b) Batten, S. R.; Hoskins, B. F.; Robson, R. *Angew. Chem., Int. Ed. Engl.* **1995**, *34*, 820. (c) Yaghi, O. M.; Li, G.; Li, H. *Nature* **1995**, *378*, 703. (d) Yaghi, O. M.; Li, H. *J. Am. Chem. Soc.* **1996**, *118*, 295. (e) Real, J. A.; Andrés, E.; Munoz, M. C.; Julve, M.; Granier, T.; Bousseksou, A.; Varret, F. *Science* **1995**, *268*, 265.

S0020-1669(97)00964-6 CCC: $15.00
Published on Web 01/01/1998

we report an approach to the two-step synthesis of extended structures. This involves the isolation of solvated polynuclear building blocks, followed by their desolvation leading to the extended structures.

Five discrete oligomeric complexes derived from the reaction between $[Mn(BS)(H_2O)]ClO_4$ and $[NEt_4]_3[Fe(CN)_6]$ have been isolated; they are a dinuclear complex $[NEt_4]_2[Mn(saldmen)(H_2O)][Fe(CN)_6]$, **1**, three trinuclear complexes *rac*-$[NEt_4][Mn(salmen)(MeOH)]_2[Fe(CN)_6]$, **2**, *rac*-$[NEt_4][Mn(salcy)(MeOH)]_2[Fe(CN)_6]$, **3**, and (*R*,*R*)-$[NEt_4][Mn(salcy)(H_2O)]_2[Fe(CN)_6]$, **4**, and a pentanuclear complex $[Mn(saltmen)(H_2O)]_4[Fe(CN)_6]ClO_4$, **5** (see Scheme 1 for abbreviations).

The X-ray analyses for **1** and **2** showed that the dinuclear and trinuclear units are held together and are magnetically diluted by a network of hydrogen bonding due to the presence of coordinated and free solvent molecules like H_2O and MeOH in the structure. The desolvation of **1**−**5** has been carried out for evaluating whether or not the loss of solvent in the solid state would produce extended structures with significant differences in the magnetic properties. A comparison of the magnetic properties between solvated and desolvated species is reported here.

Scheme 1

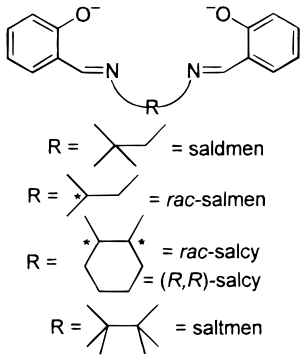

Experimental Section

Physical Measurements. Elemental analyses for C, H, and N were performed at the Elemental Analysis Service Center of Kyushu University. Manganese and iron analyses were made on a Shimadzu AA-680 atomic absorption/flame emission spectrophotometer. Infrared spectra were measured on KBr disks with JASCO IR-810 and Shimadzu FTIR-8600 spectrophotometers. Densities were measured by the floatation method in mixed solutions of benzene and tetrachloromethane. Thermogravimetric analyses (TGA) were carried out by a Rigaku Denki TG-DTA apparatus, where the heating rate was 2.5 °C/min and the temperature range was 20−300 °C. Magnetic susceptibilities were preliminary measured with a Faraday balance in the temperature range 80−300 K and with a HOXSAN HSM-D SQUID magnetic susceptometer under the applied magnetic field of 100 Oe in the 4.2−100 K temperature range at Kyushu University. The calibrations were made with $[Ni(en)_3]S_2O_3$ (en = ethylenediamine) for the Faraday balance and with $Mn(NH_4)_2(SO_4)_2\cdot 6H_2O$ for the SQUID susceptometer.[6] Magnetic susceptibilities were ultimately measured at Lausanne University using a MPMS5 SQUID susceptometer (Quantum Design Inc.), where the temperature range is 1.9−300 K and the applied magnetic fields were 600−1000 G. Field dependences of magnetization up to 5.5 kOe, field-cooled magnetization measurements, and a hysteresis loop were made on the MPMS5 SQUID susceptometer. Corrections were applied for diamagnetism, calculated from Pascal's constants.[7] Effective magnetic moments were calculated by the equation $\mu_{eff} = 2.828(\chi_M T)^{1/2}$, where χ_M is the magnetic susceptibility per formula unit. Fitting of the magnetic data to the theoretical expression was performed by minimizing the agreement factor defined as $F = \sum_i(\chi_i^{obsd} - \chi_i^{calcd})^2/\chi_i^{obsd}$ through a Levenberg−Marquart routine.[8]

X-ray Data Collection, Reduction, and Structure Determination. Single crystals of **1** and **2** were prepared by allowing the solution to stand for several days. The crystals of **1** and **2** were cut from thin plate crystals, mounted on glass fibers and coated with epoxy resin. Crystal dimensions are 0.2 × 0.2 × 0.3 mm for **1** and 0.25 × 0.2 × 0.3 mm for **2**. All measurements were made on a Rigaku AFC7R diffractometer with graphite-monochromated Mo Kα radiation (λ = 0.710 69 Å) and a 12 kW rotating anode generator. The data were collected at a temperature of 20 ± 1 °C using $\theta-2\theta$ scan technique to a maximum 2θ value of 50.0° at a scan speed of 16.0 deg/min. The weak reflections ($I < 10.0\sigma(I)$) were rescanned (maximum of four scans) and the counts were accumulated to ensure good counting statistics. Stationary background counts were recorded on each side of the reflection. The ratio of peak counting time to background counting time was 2:1. The diameter of the incident beam collimator was 1.0 mm, the crystal to detector distance was 235 mm, and the computer-controlled detector aperture was set to 9.0 × 13.0 mm (horizontal vertical). The intensities of three representative reflections

(2) (a) Miller, J. S.; Epstein, A. J.; Reiff, W. M. *Chem. Rev.* **1988**, *88*, 201. (b) Nakatani, K.; Carriat, J. Y.; Journaux, Y.; Kahn, O.; Lloret, F.; Renard, J. P.; Pei, Y.; Sletten, J.; Verdaguer, M. *J. Am. Chem. Soc.* **1989**, *111*, 5739. (c) Kahn, O.; Pei, Y.; Verdaguer, M.; Renard, J. P.; Sletten, J. *J. Am. Chem. Soc.* **1988**, *110*, 782. (d) Caneschi, A.; Gatteschi, D.; Renard, J. P.; Rey, P.; Sessoli, R. *Inorg. Chem.* **1989**, *28*, 1976. (e) Caneschi, A.; Gatteschi, D.; Renard, J. P.; Rey, P.; Sessoli, R. *Inorg. Chem.* **1989**, *28*, 3314. (f) Caneschi, A.; Gatteschi, D.; Rey. P.; Sessoli, R. *Inorg. Chem.* **1991**, *30*, 3937. (g) Benelli, C.; Caneschi, A.; Gatteschi, D.; Sessoli, R. *Inorg. Chem.* **1993**, *32*, 4797. (h) Caneschi, A.; Gatteschi, D.; Sessoli, R. *Inorg. Chem.* **1993**, *32*, 4612. (i) Gatteschi, D. *Adv. Mater.* **1994**, *6*, 635. (j) Caneschi, A.; Gatteschi, D.; Sessoli, R.; Rey, P. *Acc. Chem. Res.* **1989**, *22*, 392. (k) Caneschi, A.; Gatteschi, D.; Rey, P. *Prog. Inorg. Chem.* **1989**, *22*, 392. (l) Miller, J. S.; Epstein, A. J. *Angew. Chem., Int. Ed. Engl.* **1994**, *106*, 399. (m) Lorente, M. A. M.; Tuchagues, J. P.; Petrouleas, V.; Savariault, J. M.; Poinsot, R.; Drillon, M. *Inorg. Chem.* **1991**, *30*, 3587. (n) Stumpf, H. O.; Pei, Y.; Kahn, O.; Sletten, J.; Renard, J. P. *J. Am. Chem. Soc.* **1993**, *115*, 6738. (o) Stumpf, H. O.; Ouahab, L.; Pei, Y.; Grandjean, D.; Kahn, O. *Science* **1993**, *261*, 447. (p) Tamaki, H.; Zhong, Z. J.; Matsumoto, N.; Kida, S.; Koikawa, M.; Achiwa, N.; Hashimoto, Y.; Okawa, H. *J. Am. Chem. Soc.* **1992**, *114*, 6974. (q) Ohba, M.; Maruono, N.; Okawa, H.; Enoki, T.; Latour, J.-M. *J. Am. Chem. Soc.* **1994**, *116*, 11567. (r) Ohba, M.; Okawa, H.; Ito, T.; Ohto, A. *J. Chem. Soc., Chem. Commun.* **1995**, 1545. (s) Inoue, K.; Iwamura, H. *J. Am. Chem. Soc.* **1994**, *116*, 3173. (t) Grieber, W. D.; Babel, D. *Z. Naturforsch.* **1982**, *87b*, 832. (u) Gadet, V.; Mallah, T.; Castro, I.; Veillet, P.; Verdaguer, M. *J. Am. Chem. Soc.* **1992**, *114*, 9213. (v) Mallah, T.; Thiebault, S.; Verdaguer, M.; Veillet, P. *Science* **1993**, *262*, 1555. (w) Mitra, S.; Gregson, A. K.; Hatfield, W. E.; Weller, R. R. *Inorg. Chem.* **1983**, *22*, 1729. (x) Martinez-Lorente, M. A.; Tuchagues, J. P.; Pétrouléas, V.; Savariault, J. M.; Poinsot, R.; Drillon, M. *Inorg. Chem.* **1991**, *30*, 3587.

(3) (a) Kahn, O. *Molecular Magnetism*, VCH Verlagsgesellschaft: Weinheim, Germany, 1993. (b) Kahn, O. *Structure and Bonding*; Springer: Berlin-Heidelberg, 1987; Vol. 68. (c) *Magnetic Molecular Materials*; Gatteschi, D., Kahn, O., Miller, J. S., Palacio, F., Eds.; NATO ASI Series E; Kluwer Academic: Dordrecht, Holland, 1991; Vol. 198. (d) *Magneto-Structural Correlations in Exchange Coupled System*; Willett, R. D., Gatteschi, D., Kahn, O., Eds.; Nato ASI Series C; Kluwer Academic: Dordrecht, Holland, 1985; Vol. 140. (e) Miller, J. S.; Epstein, A. J. *Angew. Chem., Int. Ed. Engl.* **1994**, *33*, 385. (f) Borrás-Almenar, J. J.; Coronado, E.; Curely, J.; Georges, R; Gianduzzo, J. C. *Inorg. Chem.* **1994**, *33*, 5171. (g) Gleizes, A.; Verdaguer, M. *J. Am. Chem. Soc.* **1984**, *106*, 3727.

(4) (a) Sato, O.; Iyoda, T.; Fujishima, A.; Hashimoto, K. *Science* **1996**, *272*, 704. (b) Hinek, R.; Guetlich, P.; Hauser, A. *Inorg. Chem.* **1994**, *33*, 567.

(5) (a) Miyasaka, H.; Matsumoto, N.; Okawa, H.; Re, N.; Gallo, E.; Floriani, C. *Angew. Chem., Int. Ed. Engl.* **1995**, *34*, 1446. (b) *J. Am. Chem. Soc.* **1996**, *118*, 981. (c) Re, N.; Gallo, E.; Floriani, C.; Miyasaka, H.; Matsumoto, N. *Inorg. Chem.* **1996**, *35*, 6004. (d) Miyasaka, H.; Matsumoto, N.; Re, N.; Gallo, E.; Floriani, C. *Inorg. Chem.* **1997**, *36*, 670.

(6) Lindoy, L. F.; Katovic, V.; Busch, D. H. *J. Chem. Educ.* **1972**, *49*, 117.

(7) Boudreaux, E. A.; Mulay, L. N. In *Theory and Applications of Molecular Paramagnetism*; Wiley: New York, 1976; pp 491−495.

(8) Press, W. H.; Flannery, B. P.; Teukolsky, S. A.; Vetterling, W. T. *Numerical Recipes*; Cambridge University Press: Cambridge, U.K., 1989.

Table 1. Experimental Data for the X-ray Diffraction Studies on Crystalline Complexes **1** and **2**

	1	**2**
formula	$C_{41}H_{72}FeMnN_{10}O_8$	$C_{50}H_{60}FeMn_2N_{11}O_6$
fw	943.87	1076.82
space group	$P2_1/m$	$Pbcn$
a/Å	11.371(2)	15.960(3)
b/Å	19.035(2)	15.534(5)
c/Å	11.956(1)	21.798(6)
α/deg	90	90
β/deg	100.78(1)	90
γ/deg	90	90
V/Å^3	2542.2(5)	5403(3)
Z	2	4
D_m[a]/g cm^{-3}	1.23	1.36
D_c/g cm^{-3}	1.233	1.323
μ(Mo Kα)/cm^{-1}	5.88	7.81
R[b]	8.6	7.6
R_w[c,d]	9.6	7.1

[a] Determined by floatation method in benzene/tetrachloromethane. [b] $R = \sum||F_o| - |F_c||/\sum|F_o|$. [c] $R_w = [\sum w(|F_o| - |F_c|)^2/\sum w|F_o|^2]^{1/2}$. [d] $w = 1/\sigma^2(|F_o|)$.

were measured after every 150 reflections. Over the course of data collection, standard reflections were monitored and the decay corrections were applied by a polynomial correction. An empirical absorption correction based on azimuthal scans of several reflections was used. The data were corrected for Lorentz and polarization effects.

The structures were solved by direct methods[9] and expanded using Fourier techniques.[10] The non-hydrogen atoms were refined anisotropically. Hydrogen atoms were included at calculated coordinates with fixed parameters. Full-matrix least-squares refinement based on observed reflections ($I > 3.00\sigma(I)$) was employed, where the unweighted and weighted agreement factors of $R = \sum||F_o| - |F_c||/\sum|F_o|$ and $R_w = [\sum w(|F_o| - |F_c|)^2/\sum w|F_o|^2]^{1/2}$ are used. The weighting scheme was based on counting statistics. Plots of $\sum w(|F_o| - |F_c|)^2$ versus $|F_o|$, reflection order in data collection, sin θ/λ, and various classes of indices showed no unusual trends. Neutral-atom scattering factors were taken from Cromer and Waber.[11] Anomalous dispersion effects were included in F_{calcd}; the values $\Delta f'$ and $\Delta f''$ were those of Creagh and McAuley.[12] The values for the mass attenuation coefficients are those of Creagh and Hubbel. [13] All calculations were performed using the teXsan crystallographic software package of Molecular Structure Corp.[14] Crystal data and details of the structure determinations of **1** and **2** are summarized in Table 1.

General Procedures and Materials. All chemicals and solvents were reagent grade. The quadridentate Schiff base ligands *rac*-H_2salmen, H_2saldmen, *rac*-H_2salcy, (*R*,*R*)-H_2salcy, and H_2saltmen were prepared by mixing the corresponding salicylaldehyde and the diamine in a 2:1 mol ratio in ethanol, according to the literature.[15] $[NEt_4]_3[Fe(CN)_6]$ was prepared according to the literature.[16] Since the hexacyanometalate ion has a tendency to decompose on heating or irradiation, the syntheses of the manganese(III)−iron(III) complexes were performed at room temperature and the crystallization was performed in a dark room.

Caution: Perchlorate salts are potentially explosive and should only be handled in small quantities.

Precursor Manganese(III) Complexes [Mn(BS)(S)]ClO_4 or [Mn(BS)(S)$_2$]ClO_4 (H_2(BS) = H_2saldmen, *rac*-H_2salmen, *rac*-H_2salcy, (*R*,*R*)-H_2salcy, H_2saltmen, S = H_2O). The manganese(III) complexes were prepared by mixing manganese(III) acetate dihydrate, H_2BS, and $NaClO_4$ in methanol/H_2O with the molar ratio of 1:1:1.5, according to the method reported previously.[17] The complexes were obtained as dark brown crystals and were characterized by C, H, and N microanalyses and by the characteristic bands in their IR spectra.

$[NEt_4]_2$[Mn(saldmen)(H_2O)][Fe(CN)$_6$] (1). To the solution of [Mn(saldmen)(H_2O)]ClO_4 (0.233 g, 0.5 mmol) in methanol (50 mL) was added a solution of $[NEt_4]_3[Fe(CN)_6]$ (0.301 g, 0.5 mmol) in methanol (10 mL). After the reaction mixture was stirred for 10 min, 2-propanol (30 mL) was added to the dark brown solution and then the mixture filtered. The filtrate was kept for 3 days, and dark reddish-brown rectangular crystals formed. These crystals were collected by suction filtration, washed with a minimum amount of 2-propanol, and dried *in vacuo* to give the brown powder samples. The crystals for X-ray crystallography were used without drying *in vacuo* and contained one water and one methanol molecule as solvents of crystallization. Anal. Calcd for $C_{40}H_{58}N_{10}O_2MnFe$: C, 58.47; H, 7.11; N, 17.05; Mn, 6.69; Fe, 6.80. Found: C, 58.58; H, 7.09; N, 17.02; Mn, 6.26; Fe, 5.44. IR (KBr): $\nu_{C=N}$(imine) 1616 cm^{-1} (br); $\nu_{C\equiv N}$(cyanide) 2104 cm^{-1}.

***rac*-$[NEt_4]$[Mn(salmen)(MeOH)]$_2$[Fe(CN)$_6$] (2).** To a solution of *rac*-[Mn(salmen)(H_2O)]ClO_4 (226 g, 0.5 mmol) in methanol (30 mL) was added a solution of $[NEt_4]_3[Fe(CN)_6]$ (0.301 g, 0.5 mmol) in methanol (10 mL). The dark brown solution was stirred for 10 min, and to this mixture was added ethanol (60 mL). The resulting solution was stirred again for 10 min and then filtered. The filtrate was kept for 4 days and gave dark reddish-brown rectangular crystals, which were collected by suction filtration, washed with the minimum volume of ethanol, and dried *in vacuo*. These crystals were suitable for X-ray crystallography. Anal. Calcd for $C_{50}H_{60}FeN_{11}Mn_2O_6$: C, 55.77; H, 5.62; Fe, 5.19; Mn, 10.20; N, 14.31. Found: C, 56.08; H, 5.75; Fe, 4.26; Mn, 9.71; N, 13.98. IR (KBr): $\nu_{C=N}$(imine) 1601, 1624 cm^{-1}; $\nu_{C\equiv N}$(cyanide) 2106 (sh), 2120 cm^{-1}. TGA−DTA: 105−135 °C (2MeOH) and 205 °C (dec).

***rac*-$[NEt_4]$[Mn(salcy)(MeOH)]$_2$[Fe(CN)$_6$] (3).** To a solution of *rac*-[Mn(salcy)(H_2O)$_2$]ClO_4 (0.255 g, 0.5 mmol) in methanol (50 mL) was added a solution of $[NEt_4]_3[Fe(CN)_6]$ (0.301 g, 0.5 mmol) in methanol (10 mL), and the dark brown solution was stirred for 10 min. The resulting solution was filtered off, and the filtrate was kept overnight from which dark brown needle-type crystals were obtained. These crystals were collected by suction filtration, washed with a minimum volume of ethanol, and dried *in vacuo*. Anal. Calcd for $C_{56}H_{68}FeMn_2N_{11}O_6$: C, 58.14; H, 5.92; Fe, 4.83; Mn, 9.50; N, 13.31. Found: C, 58.31; H, 5.98; Fe, 3.84; Mn, 9.05; N, 13.33. IR(KBr): $\nu_{C=N}$(imine) 1601, 1622 cm^{-1}; $\nu_{C\equiv N}$(cyanide) 2112 cm^{-1}. TGA−DTA: 80−110 °C (2MeOH) and 220 °C (dec).

(*R*,*R*)-$[NEt_4]$[Mn(salcy)(H_2O)]$_2$[Fe(CN)$_6$]·MeOH (4). To a solution of (*R*,*R*)-[Mn(salcy)(H_2O)$_2$]ClO_4 (255 mg, 0.5 mmol) in methanol (50 mL) was added a solution of $[NEt_4]_3[Fe(CN)_6]$ (301 mg, 0.5 mmol) in methanol (10 mL), and the dark brown solution was stirred for 10 min. The resulting solution was filtered off and the filtrate was kept overnight to give dark brown needles. These crystals were collected by suction filtration, washed with a minimum volume of ethanol, and dried *in vacuo*. Anal. Calcd for $C_{55}H_{68}$ $FeMn_2N_{11}O_7$: C, 56.90; H, 5.90; Fe, 4.81; Mn, 9.46, N, 13.27. Found: C, 56.53; H, 5.70; Fe, 4.39; Mn, 10.05; N, 13.37. IR(KBr): $\nu_{C=N}$(imine) 1601, 1622 cm^{-1}; $\nu_{C\equiv N}$(cyanide) 2112 cm^{-1}. TGA−DTA: 35−100 °C (MeOH), 110−130 °C (2H_2O), and 200 °C (dec).

[Mn(saltmen)(H_2O)]$_4$[Fe(CN)$_6$]ClO_4 (5). To a solution of [Mn(saltmen)(H_2O)]ClO_4 (0.247 g, 0.5 mmol) in ethanol (30 mL) was added a solution of $[NEt_4]_3[Fe(CN)_6]$ (301 mg, 0.5 mmol) in ethanol (10 mL).

(9) Sheldrick, G. M. *SHELXS*86: *A program for X-ray crystal structure determination*; University of Cambridge: Cambridge, England, 1986.
(10) DIRDIF92: Beurskens, P. T.; Admiraal, G.; Beurskens, G.; Bosman, W. P.; Garcia-Granda, S.; Gould, R. O.; Smits, J. M. M.; Smykalla, C. *The DIRDIF program system*. Technical Report of the Crystallography Laboratory; University of Nijmegen: Nijmegen, The Netherlands, 1992.
(11) Cromer, D. T.; Waber, J. T. *International Tables for Crystallography*; The Kynoch Press: Birmingham, England, 1974; Vol. IV, Table 2.2A.
(12) Creagh, D. C.; McAuley, W. J. In *International Tables for Crystallography*; Wilson, A. J. C., Ed.; Kluwer: Boston, 1992; Vol. C, pp 219−222, Table 4.2.6.8.
(13) Creagh, D. C.; Hubbel, J. H. In *International Tables for Crystallography*; Wilson, A. J. C., Ed.; Kluwer: Boston, 1992; Vol. C, pp 200−206, Table 4.2.4.3.
(14) *teXsan: Crystal Structure Analysis Package*, Molecular Structure Corp.: The Woodlands, TX, 1985, 1992.
(15) Pfeifer, P.; Hesse, T.; Pfitzner, H.; Scholl, W.; Thielert, H. *J. Prakt. Chem.* **1937**, *149*, 217.
(16) Mascharak, P. K. *Inorg. Chem.* **1986**, *25*, 245.
(17) Matsumoto, N.; Takemoto, N.; Ohyoshi, A.; Okawa, H. *Bull. Chem. Soc. Jpn.* **1988**, *61*, 2984.

Scheme 2

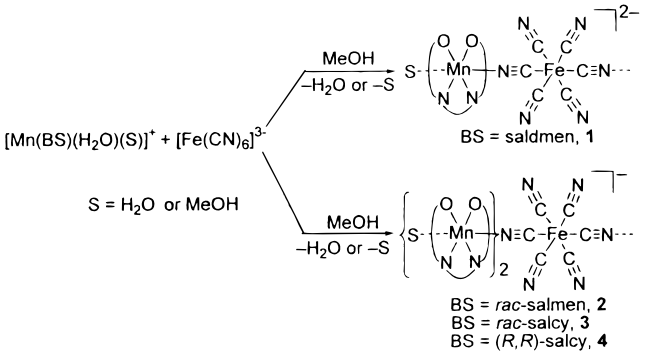

The resulting solution was stirred for 10 min, and the resulting yellowish-brown precipitate was collected by suction filtration, washed with a minimum volume of ethanol, and dried *in vacuo*. Anal. Calcd for $C_{86}H_{96}ClFeMn_4N_{14}O_{16}$: C, 54.57; H, 5.11; Fe, 2.95; Mn, 11.61; N, 10.36. Found: C, 54.37; H, 5.14; Fe, 2.38; Mn, 11.20; N, 10.27. IR(KBr): $\nu_{C=N}$(imine) 1603 cm^{-1}; $\nu_{C\equiv N}$(cyanide) 2116 cm^{-1}, ν_{Cl-O}(ClO_4), 1096 cm^{-1} (br). TGA−DTA: 30−115 °C($4H_2O$) and ca. 205 °C(dec).

Desolvated Samples 1′−5′ of 1−5. Thermogravimetric analysis (TGA) and differential thermal analysis (DTA) were carried out in the temperature range 20−300 °C with a heating rate of 2.5 °C/min; the weight losses corresponding to the crystal solvent molecules expected from the microanalyses were observed. The desolvated samples were prepared through the thermal analysis procedure, where the sample weight is ca. 15 mg for each run, the heating rate is 2.5 °C/min, and the maximum temperature was 150 °C. The IR band assigned to $\nu_{C\equiv N}$(cyanide) was observed at 2104, 2108, 2106, 2106, and 2116 cm^{-1} for **1′**, **2′**, **3′**, **4′**, and **5′**, respectively.

Results and Discussion

Synthesis and Characterization. Complexes [Mn(BS)(H_2O)]$^+$ and $[Fe(CN)_6]^{3-}$ assemble differently, depending on the Schiff-base ligand, their counterions, and the reaction solvents. The choice of the solvent is dictated by the necessity of carrying out the reaction in a homogeneous phase, thus the two factors are, in fact, interrelated, as it has been shown in related syntheses.[5a,b] When the reaction between [Mn(BS)(H_2O)]ClO_4 and $K_3[Fe(CN)_6]$ was carried out in a water−methanol mixture, multidimensional extended structures were obtained. Due to the greater solubility of $(NEt_4)_3[Fe(CN)_6]$ in organic solvents, we were able to perform the reaction with [Mn(BS)(H_2O)]ClO_4 in methanol or ethanol. The reactions produce dinuclear (**1**), trinuclear (**2**−**4**) (Scheme 2), and pentanuclear (**5**) (Scheme 3) complexes, depending on the ligand nature and regardless of the stoichiometric ratio, which was kept constant (1:1) for all of the reactions.

According to the microanalyses, each compound of the **1**−**5** series contains a water or methanol molecule filling the remaining coordination site at manganese. The single infrared band due to C≡N at 2118 cm^{-1} in $[NEt_4]_3[Fe(CN)_6]$ splits into two bands for **2** (2120 and 2106 cm^{-1}), while a single band was observed at 2104, 2112, 2112, and 2116 cm^{-1} for **1**, **3**, **4**, and **5**, respectively.

The X-ray analysis carried out on **1** and **2** (*vide infra*) shows that such molecules with other methanol/water as solvents of crystallization establish an extended network where the different discrete complexes are hydrogen bonded to each other (see Schemes 4 and 5 for **1** and **2**, respectively) but do not show any magnetic communication. The solvent molecules can be, however, removed by heating to create direct communication between the polynuclear building blocks, without the intermediacy of the solvent (Scheme 6). Desolvation was carried out

Scheme 3

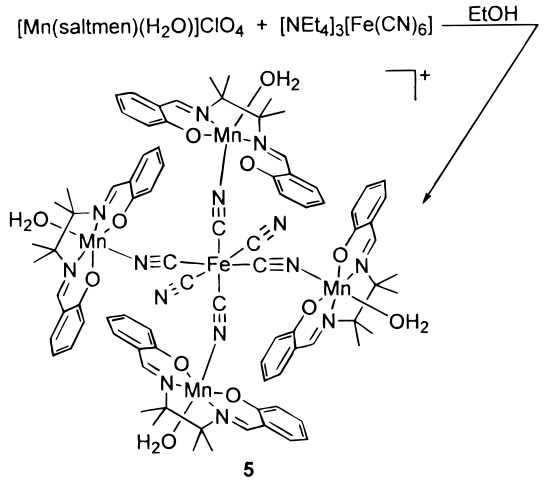

Scheme 4

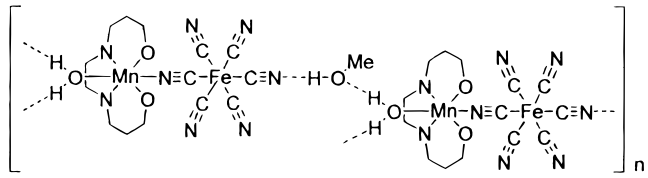

Scheme 5

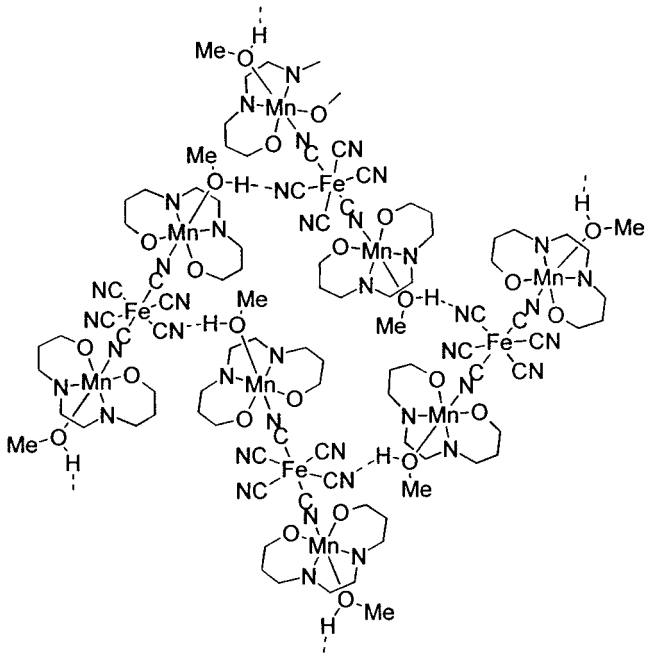

gradually from room temperature to 180 °C, the decomposition temperature being 205−220 °C (see details of the TGA−DTA data in the Experimental Section). The thermal analysis in the case of **2** showed the complete loss of MeOH at *ca.* 130 °C. This procedure has been applied to obtain all of the desolvated **1′**−**5′** forms.

Structural Analysis of 1. An ORTEP drawing of [(H_2O)-Mn(saldmen)Fe$(CN)_6]^{2-}$ with the atom-numbering scheme is given in Figure 1. Relevant interatomic bond distances and angles are listed in Table 2. The crystal consists of the dianion [(H_2O)Mn(saldmen)Fe$(CN)_6]^{2-}$, two tetraethylammonium cations, and water and methanol as crystallization solvents in 2:1 mol ratio. Since the space group is $P2_1/m$ and the unit cell contains two dinuclear molecular units, the asymmetrical unit

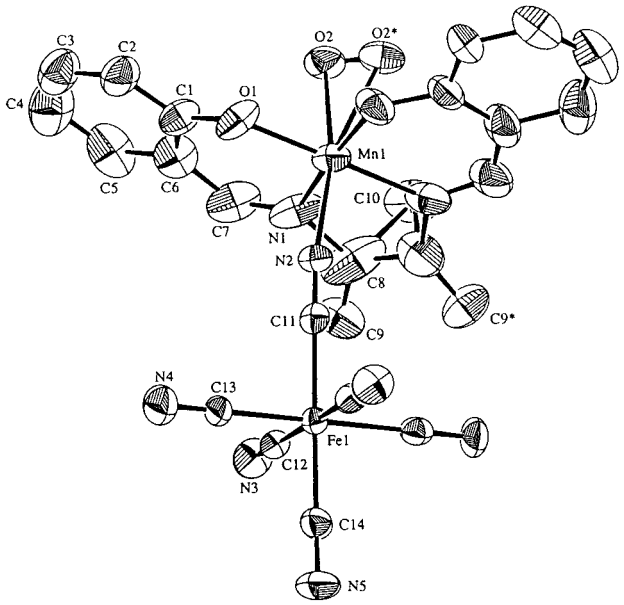

Figure 1. ORTEP drawing of **1** (50% probability ellipsoids).

Scheme 6

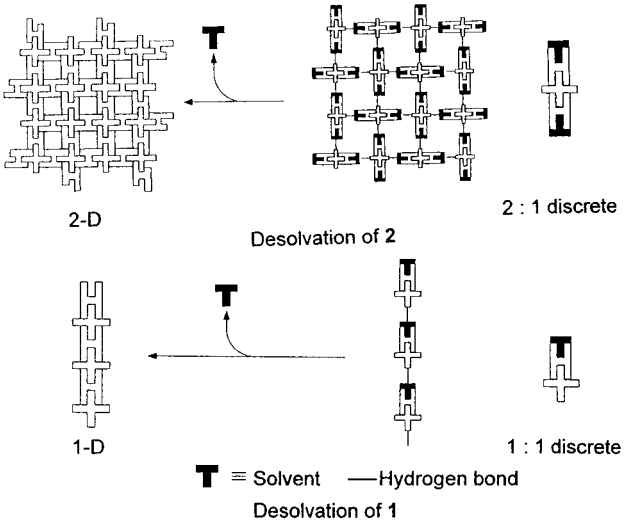

is one-half of a dinuclear unit in which a mirror plane is running through the atoms of Mn, Fe, C(11), C(14), N(2), N(5), and C(10) and bisects the binuclear molecule.

One CN^- group of the $Fe(CN)_6^{3-}$ moiety bridges to the Mn ion to give a μ-CN Mn(III)−Fe(III) structure with bond distances of Fe−C(11) = 1.93(1) Å, Mn−N(2) = 2.198(9) Å, and C(11)−N(2) = 1.15(1) Å and angles of Fe−C(11)−N(2) = 177.6(8)° and C(11)−N(2)−Mn = 162.4(8)°. The coordination geometry around Mn is an elongated square bipyramid in which the equatorial sites are occupied by N_2O_2 donor atoms of the quadridentate Schiff-base ligand saldmen^{2-} with one of the two apical sites occupied by a cyanide group of $[Fe(CN)_6]^{2-}$ and the other site occupied by a water molecule with a Mn−O(2) distance of 2.370(9) Å.[18]

Figure 2 shows a molecular packing diagram of the binuclear units of **1** projected onto the *ac* plane and the hydrogen-bonding

(18) The water molecule is disordered over two positions related by the O2 and O2* mirror plane. The two methyl groups of the 1,1′-dimethylethylenediamine fragments have an occupancy factor of 50%, thus preventing the assignment to which carbon of the ethylene bridge they are bonded to.

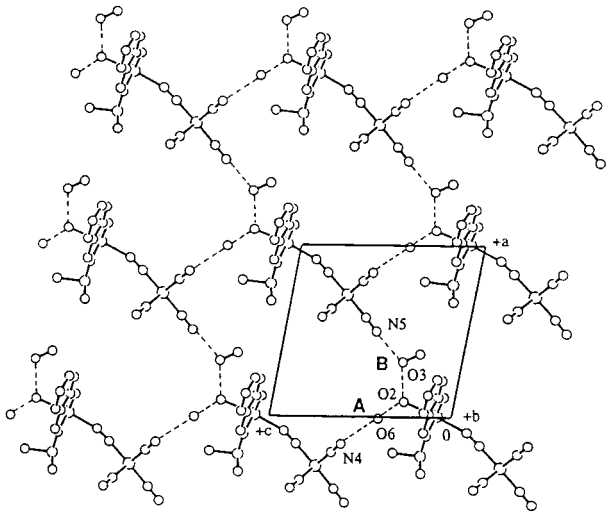

Figure 2. Projection along the *b*-axis of **1**, showing a network structure formed by hydrogen bonds.

Table 2. Relevant Bond Distances (Å), Bond Angles (deg), and Hydrogen Bonds (Å) of **1**

Bond Distances			
Fe(1)−C(11)	1.93(1)	Fe(1)−C(12)	1.986(8)
Fe(1)−C(13)	1.907(8)	Fe(1)−C(14)	1.90(1)
Mn(1)−O(1)	1.881(6)	Mn(1)−O(2)	2.370(9)
Mn(1)−N(1)	1.987(8)	Mn(1)−N(2)	2.198(9)
N(2)−C(11)	1.15(1)	N(3)−C(12)	1.126(8)
N(4)−C(13)	1.144(8)	N(5)−C(14)	1.15(1)
Bond Angles			
C(11)−Fe(1)−C(12)	89.9(3)	C(11)−Fe(1)−C(13)	90.3(3)
C(11)−Fe(1)−C(14)	178.0(4)	C(12)−Fe(1)−C(13)	91.6(3)
C(12)−Fe(1)−C(14)	88.7(3)	C(12)−Fe(1)−C(14)	88.7(3)
O(1)−Mn(1)−O(2)	79.8(3)	O(1)−Mn(1)−N(1)	92.7(3)
O(1)−Mn(1)−N(2)	94.3(2)	O(2)−Mn(1)−N(1)	78.0(3)
O(2)−Mn(1)−N(2)	165.2(3)	N(1)−Mn(1)−N(2)	88.7(3)
Mn(1)−N(2)−C(11)	162.4(8)		
Fe(1)−C(11)−N(2)	177.6(8)	Fe(1)−C(12)−N(3)	179.5(7)
Fe(1)−C(13)−N(4)	179.5(8)	Fe(1)−C(14)−N(5)	178(1)
Hydrogen Bonds			
O(2)···O(3)	2.60(2)	O(2)···O(6)	2.89(2)
O(3)···N(5)	2.65(2)	O(6)···N(4)	3.01(1)

network. The hydrogen bond distances range from 2.60(2) to 3.01(1) Å (O(2)···O(3) = 2.60(2) Å, O(2)···O(6) = 2.89(2), O(3)···N(5) = 2.65(2) Å, O(6)···N(4) = 3.01(1) Å).

Structural Analysis of 2. An ORTEP drawing of **2** is in Figure 3, while interatomic bond distances and angles are listed in Table 3. The crystal consists of the [(MeOH)Mn(salmen)-$Fe(CN)_6$Mn(salmen)(MeOH)]$^-$ anion and the tetraethylammonium countercation. Since the space group is *Pbcn* and the unit cell contains four trinuclear molecular units, the asymmetrical unit is one-half of a trinuclear unit and the Fe ion occupies an inversion center (0,0,0). The nitrogen atom of $[NEt_4]^+$, N(6), is in an inversion center position and the ethyl groups do not suffer from disorder.

The two CN^- groups in trans positions of the $[Fe(CN)_6]^{3-}$ moiety bridge two Mn ions, giving a linear bridging mode of Mn−NC−Fe−CN−Mn (Fe−C(19) = 1.94(1) Å, Mn−N(3) = 2.219(9) Å, C(19)−N(3) = 1.14(1) Å; Fe−C(19)−N(3) = 175.3(10)°, C(19)−N(3)−Mn = 164.7(9)°). The coordination geometry around Mn is an elongated square bipyramid in which the equatorial sites are occupied by N_2O_2 donor atoms of the Schiff base salmen while the two axial positions are filled by a cyanide ion of $[Fe(CN)_6]^{3-}$ and by a methanol molecule with a

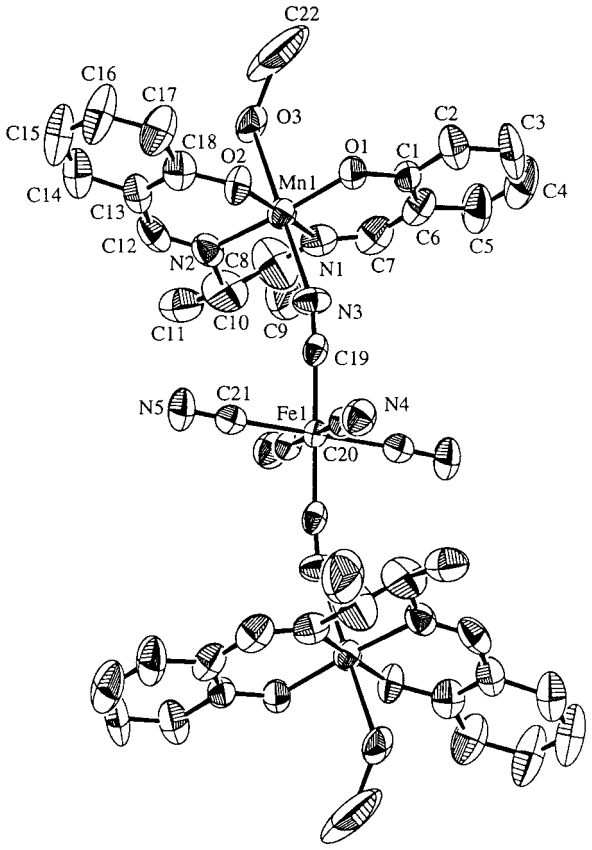

Figure 3. ORTEP drawing of **2** (30% probability ellipsoids).

Table 3. Relevant Bond Distances (Å), Bond Angles (deg), and Hydrogen Bonds (Å) of **2**

Bond Distances			
Fe(1)−C(19)	1.94(1)	Fe(1)−C(20)	1.94(1)
Fe(1)−C(21)	1.97(1)	Mn(1)−O(1)	1.877(7)
Mn(1)−O(2)	1.872(7)	Mn(1)−O(3)	2.422(7)
Mn(1)−N(1)	2.014(10)	Mn(1)−N(2)	1.987(9)
Mn(1)−N(3)	2.219(9)	N(3)−C(19)	1.14(1)
N(4)−C(20)	1.16(1)	N(5)−C(21)	1.15(1)
O(3)−C(22)	1.76(2)		
Bond Angles			
C(19)−Fe(1)−C(21)	94.2(4)	C(19)−Fe(1)−C(21)	85.8(4)
C(20)−Fe(1)−C(21)	89.1(4)		
O(1)−Mn(1)−O(3)	87.2(3)	O(2)−Mn(1)−O(3)	88.6(3)
O(1)−Mn(1)−N(3)	94.6(3)	O(2)−Mn(1)−N(3)	97.4(3)
O(3)−Mn(1)−N(1)	85.7(3)	O(3)−Mn(1)−N(2)	84.9(3)
O(3)−Mn(1)−N(3)	173.6(3)		
N(1)−Mn(1)−N(3)	88.1(4)	N(2)−Mn(1)−N(3)	92.5(4)
Mn(1)−O(3)−C(22)	120.6(7)	Mn(1)−N(3)−C(19)	164.7(9)
Fe(1)−C(19)−N(3)	175.3(10)	Fe(1)−C(20)−N(4)	176(1)
Fe(1)−C(21)−N(5)	177(1)		
Hydrogen Bonds			
O(3)···N(5)	2.79(1)		

Mn−O(3) distance of 2.422(7) Å. The trinuclear [MeO(H)-Mn−NC−Fe−CN−Mn] units are held together by a hydrogen-bonding network established by the Mn-bonded methanol (O3···N5 = 2.79(1) Å). Such an interaction led to a two-dimensional extended structure made up by the cyclic octamer $[-NC-Fe-CN-Mn-MeOH-]_4$ as a network unit (see Schemes 5 and 6). Figure 4 shows the molecular packing diagram of the trinuclear units oriented into the *ab* plane.[19]

(19) The disorder associated to the methyl substituent of the ethylene fragment does not allow the correct chirality assignment to the [Mn(salen)] moieties.

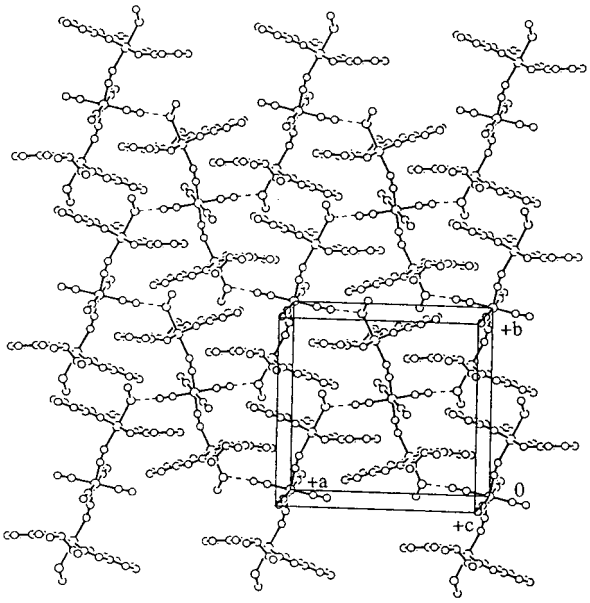

Figure 4. Projection along the *c*-axis of **2**, showing a two-dimensional network structure formed by hydrogen bonds.

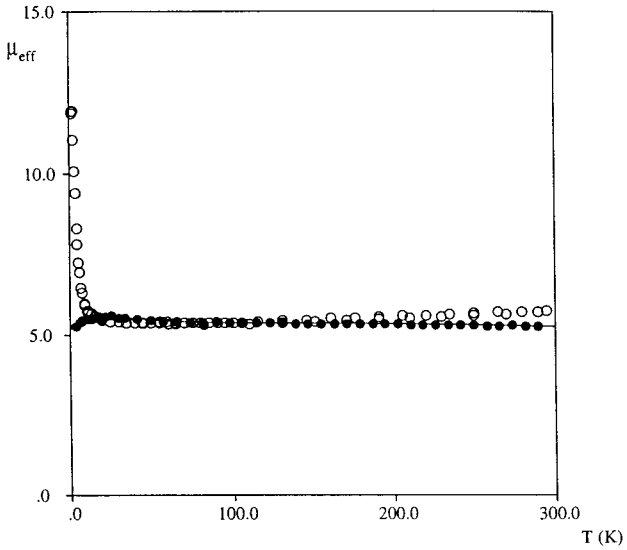

Figure 5. Effective magnetic moment μ_{eff} per MnFe *vs* *T* for **1** (●) and the desolvated sample **1′** (○).

Magnetic Properties. Complex 1. The temperature dependence of the effective magnetic moment μ_{eff} per MnFe unit is depicted in Figure 5. The μ_{eff} value at room temperature, 5.28 μ_B, is slightly larger than the spin-only value of 5.20 μ_B for the magnetically dilute two-spin system (S_{Mn}, S_{Fe}) = (2, $^1/_2$), where the spin-only value was calculated by assuming *g* values of $g_{Mn} = g_{Fe} = 2.00$. On lowering the temperature, μ_{eff} gradually increases to reach a maximum of 5.59 μ_B at 26 K and then decreases. The plot of $1/\chi_M$ *vs* *T* obeys the Curie−Weiss law $\{1/\chi_M = C/(T - \theta)\}$ with the Weiss constant $\theta = +2.0$ K, suggesting a ferromagnetic interaction between Mn(III) and Fe(III) ions through the CN group. The decrease of μ_{eff} at low temperature is due to the zero-field splitting term of the manganese(III) ion and/or an intermolecular antiferromagnetic interaction. The magnetic susceptibility data can be fit by the spin-Hamiltonian, eq 1, based on the binuclear structure with the spin system (S_{Mn}, S_{Fe}) = (2, $^1/_2$) including a zero-field splitting term for the Mn ion, *D*, and an intermolecular interaction term within the molecular field approach. The best fit

$$H = \beta H(g_{Mn}S_{Mn} + g_{Fe}S_{Fe}) - 2JS_{Mn}S_{Fe} + D[S_z^2 - S_{Mn}(S_{Mn} + 1)/3] - zJ'\langle S\rangle \quad (1)$$

parameters are $J = +4.5$ cm^{-1}, $zJ' = 0.2$ cm^{-1}, $g_{Mn} = 2.01$, $g_{Fe} = 2.05$, and $D = -9.5$ cm^{-1} (see the solid line in Figure 5).

Compounds 2, 3, and 4. The magnetic behaviors of **2**, **3**, and **4** are essentially the same, so only **2** is described here. The μ_{eff} value per Mn_2Fe *vs* T plots for **2** is depicted in Figure 6. The μ_{eff} value at room temperature is 7.05 μ_B, which is compatible with the spin-only value of 7.14 μ_B for the magnetically dilute three-spin system (S_{Mn}, S_{Fe}, S_{Mn}) = (2, $^1/_2$, 2). On lowering the temperature, the effective magnetic moment μ_{eff} for **2** gradually increases to reach a maximum of 8.49 μ_B at 6 K and then decreases slightly. The plot of $1/\chi_M$ *vs* T obeys the Curie−Weiss law, and the value of the Weiss constant θ is 3.2 K. The decrease of μ_{eff} at low temperature is due to the zero-field splitting term of the manganese(III) ion and/or an intermolecular antiferromagnetic interaction. The magnetic susceptibility data can be fit by the spin-Hamiltonian, eq 2, based on the symmetrical linear trinuclear structure of Mn(III)−Fe(III)−Mn(III) with the spin system (S_{Mn}, S_{Fe}, S_{Mn}) = (2, 1/2, 2) including a zero-field splitting term and an intermolecular interaction term within the molecular field approach, where the magnetic interaction between the terminal Mn ions is neglected.

$$H = \beta H(2g_{Mn}S_{Mn} + g_{Fe}S_{Fe}) - 2J(S_{Mn1}S_{Fe} + S_{Mn2}S_{Fe}) + D[S_z^2 - S_{Mn}(S_{Mn} + 1)/3] - zJ'\langle S\rangle \quad (2)$$

The best fit parameters are $J = +3.6$ cm^{-1}, $zJ' = -0.1$ cm^{-1}, $g_{Mn} = 1.96$, $g_{Fe} = 2.01$, and $D = -8.5$ cm^{-1} (see solid line, Figure 6).

Compound 5. The temperature dependence of the effective magnetic moment μ_{eff} per Mn_4Fe for **5** is depicted in Figure 7. The μ_{eff} value at room temperature, 10.40 μ_B, is slightly larger than the spin-only value of 9.95 μ_B for the magnetically dilute five-spin system ($S_{Mn} \times 4$, S_{Fe}) = (2×4, $^1/_2$). On lowering the temperature, the μ_{eff} value gradually decreases to reach a minimum of 9.66 μ_B at 12 K and then gradually increases to reach a maximum of 11.48 μ_B at 4.4 K. The plot of $1/\chi_M$ *vs* T obeys the Curie−Weiss law with the Weiss constant $\theta = -1.8$ K, indicating an antiferromagnetic interaction. This behavior is compatible with a discrete pentanuclear structure in which four manganese(III) Schiff-base moieties are capped by water molecule (Scheme 3).

To fit the magnetic data we first derived the theoretical expression of the magnetic susceptibility arising from the following spin hamiltonian, eq 3, in which we assumed equivalent interactions among the central iron ion and the four manganese and neglected the axial zero field splitting of the manganese centers (see Scheme 7).

$$H = \beta H(4g_{Mn}S_{Mn} + g_{Fe}S_{Fe}) - 2JS_{Fe}(S_{Mn1} + S_{Mn2} + S_{Mn3} + S_{Mn4}) \quad (3)$$

The eigenvalues of the exchange part of the hamiltonian can be easily evaluated and are given by $E(S',S) = -J[S(S + 1) - S'(S' + 1)]$, where S' and S are the total spin of the manganese centers and the total spin of the whole pentamer, respectively; $S' = S_{Mn1}+S_{Mn2}+S_{Mn3}+S_{Mn4}$, $S = S'+S_{Fe}$. Accounting for the Zeeman part of the hamiltonian through the simplified Van Vleck formula, the magnetic susceptibility can be obtained by $\chi = (N\mu_B^2/3kT)\{\sum_{S'}\sum_S g_{S,S'}2S(S + 1)(2S + 1)\exp[-E(S,S')/kT]\}/\{\sum_{S'}\sum_S(2S + 1)\exp[-E(S,S')/kT]\}$, where the $g_{S,S'}$ factors can be obtained by simple algebra.[3a,20] Although the fit is not quantitative, the agreement is remarkable for an essentially one-parameter model. In particular, the fit correctly reproduces the minimum around 15 K and the sudden increase at lower temperatures, the discrepancy being the inability to reproduce a minimum as deep as the observed one. However, the faster decrease of the magnetic moment below *ca*. 40 K could be due to the zero-field splitting of Mn(III), which is known to be relevant but is not accounted for in the model. A more rigorous theoretical treatment including this zero-field splitting has not been attempted because of the complexity of the pentanuclear

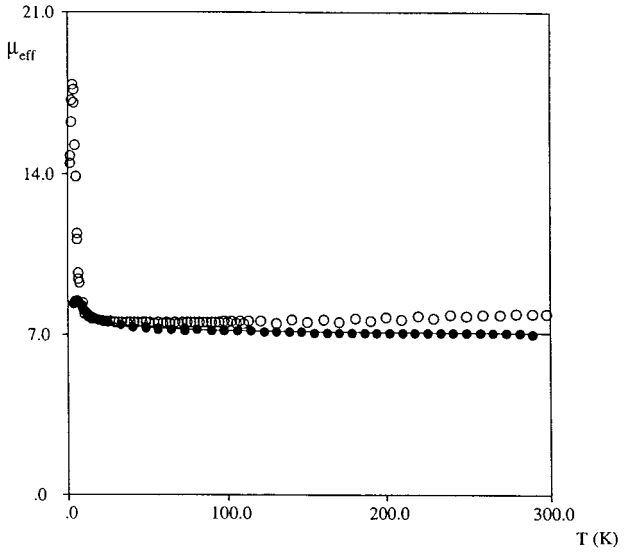

Figure 6. Effective magnetic moment μ_{eff} per Mn_2Fe *vs* T for **2** (●) and the desolvated sample **2′** (○).

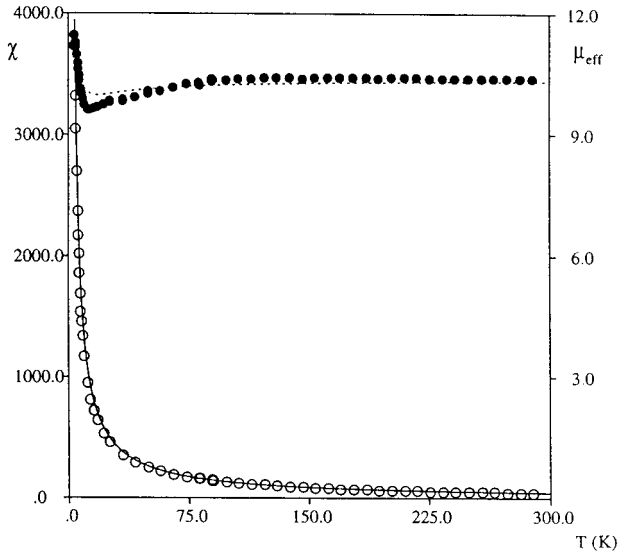

Figure 7. Magnetic susceptibility χ (○; 10^{-3} emu) and effective magnetic moment μ_{eff} (●) per Mn_4Fe *vs* T for **5**.

Scheme 7

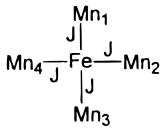

(20) Bencini, A.; Gatteschi, D. *Electronic Paramagnetic Resonance of Exchange Coupled Systems*; Springer: Berlin, Germany, 1990.

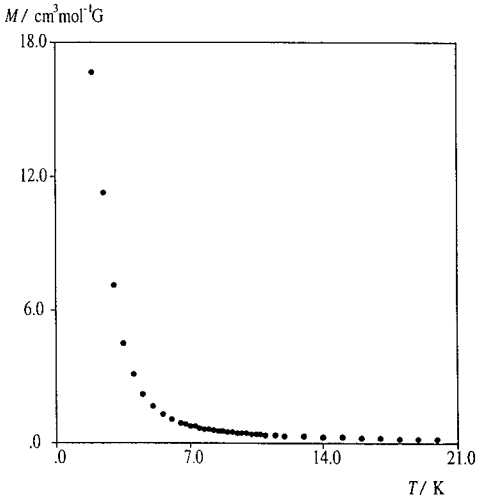

Figure 8. FCM (field-cooled magnetization *vs T*) curve under 1 Oe for **1′**.

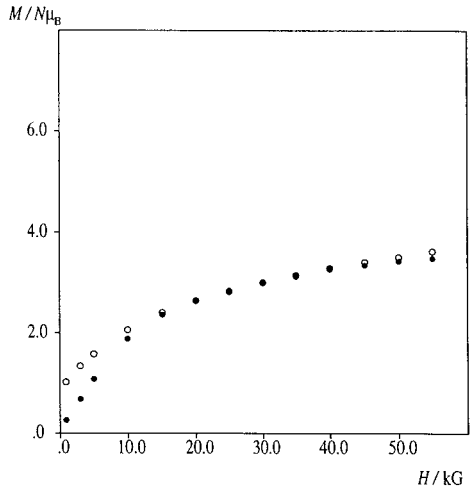

Figure 9. Magnetization as a function of the applied magnetic field performed at 1.9 K for **1** (●) and **1′** (○).

system. The best fit parameters are $J = -1.60$ cm^{-1}, $g_{Mn} = 2.08$, and $g_{Fe} = 2.2$ (see Figure 7), indicating a small antiferromagnetic interaction between Mn^{III} and Fe^{III} ions.

The structurally related complex $\{[Mn(saltmen)]_4[Fe(CN)_6]ClO_4\}_n$, which has an extended two-dimensional network structure, showed a small ferromagnetic interaction between manganese(III) and iron(III).[5] This, however, could be due to slight differences between the geometry of the pentanuclear unit in **5** and that in $[\{Mn(saltmen)\}_4\{Fe(CN)_6\}ClO_4]_n$ as a consequence of the different three-dimensional assembling.

Desolvated Compounds. The magnetic behavior of the desolvated compounds **1′**−**5′** is quite different from that of the solvated compounds described above. In particular, some of the desolvated compounds (**1′**−**3′**) show the onset of magnetic ordering indicating the formation of extended magnetic interactions.

The temperature dependence of the effective magnetic moment μ_{eff} per MnFe unit for **1′** is reported in Figure 5. Lowering the temperature results in a gradual decrease of μ_{eff} and shows a round minimum at *ca.* 60 K. It then increases abruptly to reach a value of 12.2 μ_B at 1.9 K, which is significantly higher that that of the largest possible spin state $S_T = {}^5/_2$, $\mu_{eff} = 5.92$ μ_B. The plot of $1/\chi_M$ *vs T* above 60 K obeys the Curie−Weiss law with a negative Weiss constant, $\theta = -3.2$ K, indicating the presence of an antiferromagnetic interaction. Note that the

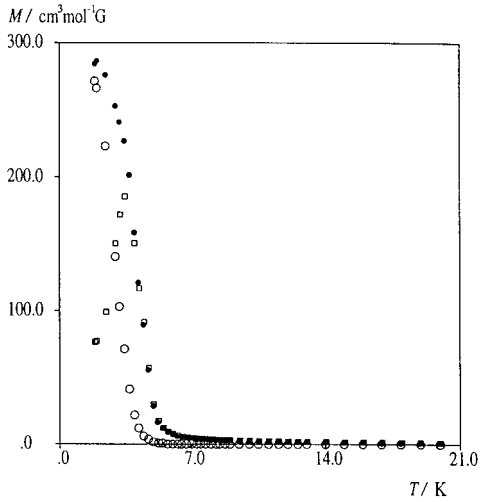

Figure 10. FCM (field-cooled magnetization *vs T*; ●) curve under 1 Oe, RM (remnant magnetization *vs T*; ○), and ZFCM (zero-field cooled magnetization; □) for **2′**.

CN-bridged coupling between Mn(III) and Fe(III) in **1′** is antiferromagnetic while the intradimer coupling in **1** is ferromagnetic. This change in the sign of the magnetic coupling is not surprising, since in analogous systems it was observed that small changes in the geometry of the Fe−C−N−Mn unit lead to significant changes and, even more, to an inversion of the magnetic coupling between the two metal ions.[5d] The sharp increase at low temperatures would suggest the onset of a three-dimensional ferrimagnetic ordering. The occurrence of a magnetic phase transition was established by measuring the magnetization as a function of the temperature under a weak magnetic field. The field-cooled magnetization (FCM) curve was obtained by cooling the sample from 20 to 1.9 K under a magnetic field of 1 Oe and shows a rapid increase below *ca.* 4 K (Figure 8). At the lowest temperature, 1.9 K, the slope of the FCM curve is still increasing so that the critical temperature (taken at the maximum of this slope) is around 1.9 K or maybe slightly lower.

The field dependence of the magnetization up to 55 kOe was measured at 1.9 K and is compared in Figure 9 with the magnetization curve for **1** taken at the same temperature. The curve of **1′** at low field has the behavior expected for a ferrimagnet with a large zero-field susceptibility, *i.e.*, a very weak magnetic field is sufficient to induce a magnetization of about 1 Nμ_B. When the field is increased further, the magnetization increases gradually and is still rising at the highest measured field (55 kOe), indicating that saturation has not yet been reached. Such a behavior is typical of systems with a relevant anisotropy due to a large zero-field splitting and is consistent with the high values observed for Mn(III) ions in analogous Schiff-base compounds.[21] However, at the highest field (55 kOe) the magnetization of **1′** reaches essentially the same value observed for **1** (3.6 and 3.5 Nμ_B, respectively) in spite of the negative coupling constant expected from the temperature dependence of the magnetic moment. This apparent discrepancy could be due to the strong magnetic anisotropy of these systems which prevents a clear magnetic saturation to be reached.

The temperature dependence of the effective magnetic moment μ_{eff} *per* Mn_2Fe unit for **2′** is shown in Figure 6. The magnetic moment at high temperatures has a value close to that of **2** (7.15 μ_B at 290 K), but as the temperature is lowered, it

(21) Kennedy, B. J.; Murray, K. S. *Inorg. Chem.* **1985**, *24*, 1552.

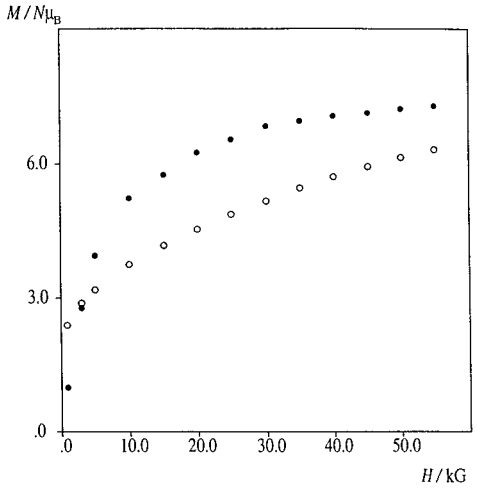

Figure 11. Magnetization as a function of the applied magnetic field performed at 1.9 K for **2** (●) and **2′** (○).

gradually decreases and shows a round minimum at *ca*. 70 K. It then sharply increases, reaching a value of 17.95 μ_B at 2.8 K, and finally decreases to 14.45 μ_B at 1.9 K. The plot of $1/\chi_M$ *vs T* above 70 K obeys the Curie−Weiss law with a negative Weiss constant, $\theta = -8.3$ K, indicating the presence of antiferromagnetic interactions. This again shows the inversion of the sign of the magnetic coupling between CN-bridged Mn(III) and Fe(III) upon desolvation. The sharp increase at low temperature would again suggest the onset of a magnetic order which is confirmed by the FCM curve taken under 1 Oe from 20 to 1.9 K (Figure 10). Here, the magnetization shows a rapid increase below *ca*. 5 K and a break in the curve around $T_c = 4$ K. When the field was switched off at 1.9 K, a remnant magnetization was observed and vanishes at T_c upon warming (Figure 10). Finally, the zero-field-cooled magnetization (ZFCM), obtained by cooling in zero field and warming under 1 Oe, was measured (Figure 10). The ZFCM curve shows a maximum at T_c, as expected for a polycrystalline ferrimagnet.

The field dependence of the magnetization up to 55 kOe was measured at 1.9 K and is compared in Figure 11 with the magnetization for **2** at the same temperature. The initial large zero-field susceptibility and the sudden increase to *ca*. 3 Nμ_B at 1 kOe (not observed for **2**) are also typical of a ferrimagnetic order. At the highest measured field (55 kOe), the magnetization of **2′** is substantially lower than that of **2** (6.3 and 7.4 Nμ_B, respectively), confirming the inversion of the magnetic coupling between the two metal ions.

The magnetic behavior of **2′** is reminiscent of what was observed for several structurally characterized two-dimensional ferri-, ferro-, or metamagnet layers containing the cyclic octamer $[-NC-Fe-CN-Mn-]_4$ (**5a**,**b**,**d**) as a building block. Such a repeating unit is quite similar to the cyclic octamer $[-NC-Fe-CN-Mn-MeOH-]_4$ present in the layer structure of **2**.

The magnetic behavior of **3′** is completely analogous to that of **2′** and will not be discussed here. The temperature dependence for **4′** and **5′** is not very different from that for **4** and **5**, respectively, and does not show any sharp increase at low temperature. Moreover, FCM studies performed on **4′** and **5′** do not show any magnetic phase transition until 1.9 K.

Conclusions

The results presented here, though limited, present an interesting synthetic methodology consisting of the assembly of polynuclear solvated building blocks *via* a thermally induced process. The solvated species already have a preorganized extended structure where the di-, tri-, and pentanuclear units are linked together by a hydrogen-bonding network. In such an extended structure, however, we do not have any magnetic communication between the different building blocks. The thermal process removes the solvent molecule of crystallization and that bonded to the metal: thus, the resulting extended structure would be obtained without a severe reorganization and with the oligomeric building blocks interacting with each other. This has been revealed by the changes in the magnetic properties of **1′**−**3′** *vs* those of the parent compounds **1**−**3**. The magnetic properties of **1′**−**3′** revealed, in fact, a magnetic ordering diagnostic of an extended structure. Such changes have been not observed moving from **4** and **5** to **4′** and **5′**. This is indicative of the limits of the synthetic methodology. The conversion of hydrogen-bonded into chemically-bonded extended structures may depend on the particular solid-state arrangement of the building blocks.

Acknowledgment. This work was supported by Ministry of Education, Science, and Culture of Japan (Grant No. 09874145) and JSPS Research Fellowships for Young Scientists (H.M.). Foundation Herbette (University of Lausanne, N.R.) and Fonds National Suisse de la Recherche Scientifique (Bern, Switzerland, Grant No. 2040268.94) are also acknowledged for financial support.

Supporting Information Available: Text giving the X-ray experimental details and tables of experimental details, atomic coordinates, anisotropic displacement parameters, and complete bond distances and angles for **1** and **2** (29 pages).

IC9709640